International Journal of Heat and Fluid Flow 29 (2008) 1319–1325

Contents lists available at ScienceDirect

International Journal of Heat and Fluid Flow

journal homepage: www.elsevier.com/locate/ijhff

Natural convective heat transfer in vertical channels with low-thermal-conductivity ribs

Giovanni Tanda *

Dipartmento di Ingegneria della Produzione, Termoenergetica e Modelli Matematici (DIPTEM/TEC), Università degli Studi di Genova, via all'Opera Pia 15/a, I-16145 Genova, Italy

ARTICLE INFO

Article history:
Received 9 January 2008
Received in revised form 6 May 2008
Accepted 19 May 2008
Available online 30 June 2008

Keywords:
Natural convection
Heat transfer
Vertical channel
Rib-roughened channel
Schlieren

ABSTRACT

The effect of repeated horizontal protrusions on the free-convection heat transfer in a vertical, asymmetrically heated, channel has been experimentally investigated. The protrusions have a square section and are made of a low-thermal-conductivity material. Experiments were conducted by varying the number of the protrusions over the heated surface (whose height was held fixed) and the aspect ratio of the channel. The convective fluid was air and the wall-to-ambient air temperature difference was set equal to 45 K. The local heat transfer coefficient was obtained by means of the schlieren optical technique.
The protrusions were found to significantly alter the heat transfer distribution along the heated surface of the channel, especially in the vicinity of each obstacle. For the ranges of parameters studied, the addition of low-conductivity protrusions leads to a decrease in the average heat transfer coefficient, as compared to that for the smooth surface, in the 0–7% range for the largest channel aspect ratio and in the 18–43% for the smallest channel aspect ratio.

1. Introduction

Natural convection in vertical channels is of interest in several technological applications (electronic equipment cooling, solar collectors, passive heating of buildings, etc.). If large-scale roughness elements are present on one or both surfaces forming the vertical channel, the buoyant flow may be significantly altered. For instance, large scale ribs can affect the free convection flow in several ways: (i) heat transfer may be reduced by the blockage effect of protrusions, (ii) disturbances in the laminar boundary layer may cause a premature transition to turbulence, and (iii) the ribs, if heated, add an extra heat transfer surface area. Establishing whether the protrusions yield heat transfer enhancement is of great importance in applications where the maximization of the heat transfer rate is the prime consideration. Moreover, there are thermal systems where the roughness occurs naturally, as in the case of an electronic circuit board with chip modules, and the knowledge of the thermal behaviour is essential for their correct design.

Several studies have been carried out to assess the influence of roughness elements on natural convection heat transfer; the results documented in the literature seem to conflict with each other, with some studies reporting increases in the heat transfer coefficient and others reporting no increases or even decreases. In previous papers, the author (Tanda, 1997; Ambrosini and Tanda, 2006) found that high-thermal-conductivity ribs led to significant decreases in the free convective heat transfer from a vertical, asymmetrically heated, channel. The same result was obtained by Bhavnani and Bergles (1990) and Acharya and Mehrotra (1993); conversely, Aydin (1997) found a slight increase (up to 10%) when the surface is ribbed. Experiments conducted in the previously mentioned papers were limited to a small range of the rib pitch-to-height ratio and within the laminar regime, therefore these results cannot be generalized in principle. The use of low-thermal-conductivity ribs or partitions (in lieu of high conductivity ones) turned out not to decrease the heat transfer (with reference to the smooth surface) and in some cases even to slightly increase it (Bhavnani and Bergles, 1990; Onbaşioğlu and Eğrican, 1998). This is probably due to the fact that the low-conductivity ribs interrupt the growing thermal boundary layer and redirect low temperature fluid flow into the near wall region.

The aim of this paper was to experimentally measure the distribution of the free-convection heat transfer coefficient along an isothermal vertical surface where transverse square ribs with low-thermal conductivity are placed. As the low-conducting ribs were held to be poorly efficient from the heat transfer point of view, no temperature or heat transfer coefficient measurements were performed along their sides. The ribbed surface was faced by a parallel, adiabatic surface to form a vertical channel whose aspect ratio (defined as the ratio between the spacing and the height) was varied in the range of 0.05–0.4.

Experiments were performed with the surface without ribs, with a single rib on the surface (in the middle), and with three or

* Tel.: +39-010-3532881; fax: +39-010-311870.
E-mail address: giovanni.tanda@unige.it

0142-727X/$ - see front matter © 2008 Elsevier Inc. All rights reserved.
doi:10.1016/j.ijheatfluidflow.2008.05.004

Nomenclature

e	rib height
h	heat transfer coefficient
H	height of the vertical surface
k	thermal conductivity of air
L	surface length
P	rib pitch
S	channel spacing
t	plate thickness
T	temperature
x	coordinate parallel to the vertical plate
y	coordinate perpendicular to the vertical plate
z	coordinate aligned to the light beam

Greek symbols

α	light ray angular deflection
Δ	light ray deviation
Ω	constant in Eq. (1)

Subscripts

y	direction perpendicular to the vertical plate
w	wall/air interface
∞	ambient air

five repeated ribs (located at regular intervals). The convective fluid was air and the experimental facility was the schlieren optical technique, properly implemented by the author in order to permit the local heat transfer coefficient reconstruction. Some preliminary results have been reported in a previous paper (Tanda, 2007), where the heat transfer characteristics of the ribbed heated plate, for two values of the wall-to-ambient air temperature difference, the channel aspect ratio being kept fixed ($S/H = 0.4$), are presented.

2. The experiments

2.1. The test section

The test section is schematically shown in Fig. 1. It consisted of a vertical plate (termed 'heated plate') made of aluminium and with an electrical resistance placed inside and two shrouding vertical walls. The shrouding walls, smooth and unheated, formed with the heated plate two adjacent, symmetrical channels. When electrical power was delivered to the resistance, owing to the high-thermal conductivity of aluminium, the heated plate attained a very uniform surface temperature at the steady state. The dimensions of the heated plate were: overall thickness (without ribs) $t = 0.012$ m, height $H = 0.175$ m, length $L = 0.3$ m. The length was set much greater than the other dimensions in order to favour a two-dimensional thermal field in the channels. The spacing S between each unheated wall and the heated plate, set equal on both sides, was varied between 8.75 and 70 mm, in order to cover a range of the channel aspect ratio S/H from 0.05 to 0.4.

Experiments were performed for the heated plate with smooth surfaces and in the presence of ribs. The ribs, made of balsa wood (thermal conductivity of 0.05 W/mK), were square in shape, with side e equal to 4.85 mm. Different ribbed surface geometries were considered, as shown in Fig. 2: with one rib per side, located at the middle of the plate, with three ribs per side (and a rib pitch P of 70 mm, $P/e = 14.4$) and with five ribs per side (rib pitch P of 35 mm, $P/e = 7.2$).

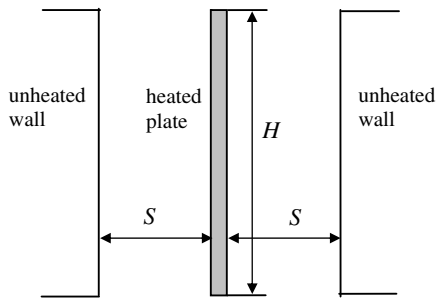

Fig. 1. Schematic view of the test section: the heated plate is vertically suspended to form, with the shrouding unheated walls, two adjacent symmetrical channels (of width S and height H).

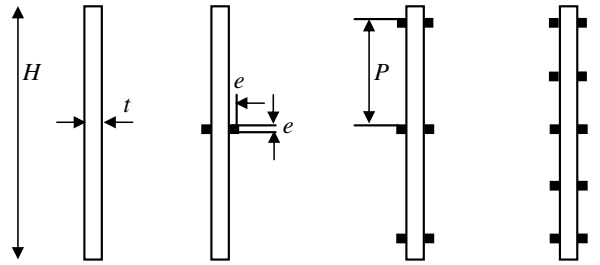

Fig. 2. Cross-sectional view of the heated plate: From left to right: plate with smooth surfaces, plate with one rib (per side), plate with three ribs (per side), $P/e = 14.4$; plate with five ribs (per side), $P/e = 7.2$. Overall height $H = 175$ mm, plate thickness $t = 12$ mm, rib side length $e = 4.85$ mm.

The advantage of having a symmetrical arrangement of the test sample (ribs on both sides) is twofold: (i) optical measurements were repeated on both sides and, owing to the symmetry, averaged at the same elevation, thus reducing the experimental error, (ii) the average of the optically obtained heat transfer coefficient was compared with that deduced by an energy balance applied to the heated plate (the power input and wall-to-fluid temperature difference being known), thus providing further support for the validity of the optical results.

Both the heated plate and the surroundings were instrumented with fine-gauge, chromel–alumel thermocouples, calibrated to ±0.1 K. Numerous thermocouples were embedded in the wall of the heated plate at different locations through 0.5-mm diameter holes drilled into the aluminium plate. Care was taken to drill the holes as close to the exposed surfaces as possible. The degree of uniformity of the surface temperature of the aluminium plate was checked by comparing the independent readings obtained in different spots (including the vertical symmetry line of the plate as well as lateral edges). For all experimental runs, the temperature readings were uniform within ±2% of the mean plate-to-ambient temperature difference. The ambient air temperature was measured by five shielded thermocouples situated just below the plate array.

For each surface geometry, tests were performed by imposing a mean heated plate-to-ambient temperature difference of 45 K. For all the experiments conducted, the buoyant air flow was laminar.

2.2. The experimental facility

A schlieren optical system was used to reconstruct the thermal field and to perform measurements of local heat transfer coeffi-

cients. The schlieren technique is based on the detection of the angular deflections that light rays undergo when crossing a non-isothermal transparent fluid; this can be accomplished by using a special filter located on the focal plane of the schlieren head (see Tanda, 1993; Devia et al., 1994; Settles, 1985, 2001). Since these deflections are related to the thermal gradients in the fluid, the local heat transfer coefficient at the wall can be easily reconstructed.

The schlieren system is schematically shown in Fig. 3a. A non-coherent light beam from a vertical slit source, collimated by the concave mirror M_1, passes through the test section. Here, the heated plate and the two shrouding vertical walls are deployed with length L aligned to the travelling light beam (i.e. along the z-coordinate of Fig. 3a). A second concave mirror, M_2, is then used to project a real image of the slit source in the focal plane and a real image of the test section onto a screen or camera. Owing to the inhomogeneities of the fluid refractive index around the heated plate, the light rays undergo angular deflections.

Regions of the optical field characterized by the same light deflection α_y in the y–z plane can be identified by shifting an opaque vertical filament in the focal plane of mirror M_2, as shown in Fig. 3b (focal filament method). When a disturbed light ray is stopped by the focal filament, the image of the corresponding region of fluid will appear dark on the screen, while the remaining field will be bright. The deflection α_y of a disturbed ray can be recorded by measuring, in the focal plane of mirror M_2, the distance Δ_y between the middle of the undisturbed image of the slit source and the centerline of the filament, i.e., the distance between filament positions 1 and 2 displayed in Fig. 3b.

It can be easily shown that distance Δ_y (corresponding to the ray shift at the focal plane of mirror M_2) is given by the product of f_2 and α_y, f_2 being the focal length of mirror M_2. If the thermal field is assumed to be two-dimensional (i.e. temperature is independent of the z-coordinate) the shift Δ_y of each light ray can be related to the local temperature gradient in the fluid by the following expression:

$$\Delta_y = \frac{\Omega}{T^2}\left(\frac{\partial T}{\partial y}\right), \tag{1}$$

where $T = T(x, y)$ is the fluid (absolute) temperature, y is the direction, normal to the heated plate, along which the light deflection is recorded, and Ω is a constant depending on the fluid, the pressure, the length of the heated plate and the geometric parameters of the optical components. In the present experiment, Ω was equal to $-0.0456\ \mathrm{m^2K}$.

A typical example of a photograph taken by the schlieren apparatus using the focal filament method is reported in Fig. 4a (heated plate with one rib per side, $\Delta_y = 1.4$ mm). By taking a number of photographs (for each experimental run) with the focal filament placed at different distances Δ_y from the undisturbed image of the slit source and by identifying, for each photograph, the coordinates of the filament shadow centerline, it is possible to obtain the

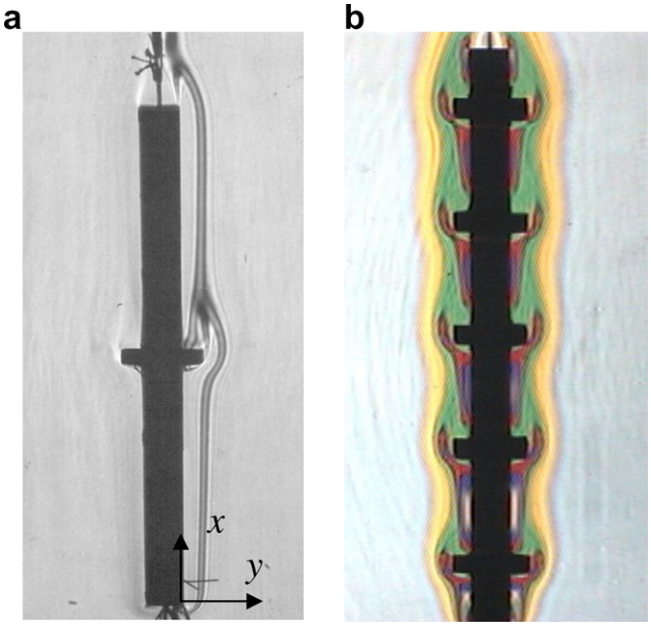

Fig. 4. Typical schlieren images: (a) filament shadow recorded for the heated plate with one rib per side ($\Delta_y = 1.4$ mm), (b) colours, identifying zones at different light angular deflections, recorded for the heated plate with five ribs per side.

pattern of lines of constant light-deviation values Δ_y and thus, applying Eq. (1), reconstruct the temperature distribution in the entire optical field. An insight of the air flow/thermal field at a glance can be obtained by using a colour filter (made of a set of thin transparent coloured strips) instead of the opaque filament mounted in the focal plane of mirror M_2. The colour schlieren method does not require any displacement of the filter. This method has the advantage of giving a whole-field image of the phenomenon without having to superimpose a number of images recorded at different time steps, as occurs with the focal filament method. Unfortunately, the measurement range is limited by the small number of coloured strips that can be mounted on the same filter; therefore colour images, like that reported in Fig. 4b (heated plate with five ribs per side), were used only for qualitative purposes (thickness of the thermal boundary layer, flow regime, etc.).

The local heat transfer coefficient can be obtained directly from schlieren images without having to reconstruct the whole thermal field. Indeed, if the focal filament is moved until its shadow intersects the vertical surface profile in the image projected on the camera, the displacement of the filament corresponds to the deviation Δ_w of the light ray passing in the vicinity of the wall at the desired location. The relation between light deviation Δ_w and the local heat transfer coefficient can be easily shown as follows. By applying Eq. (1) to the heated walls, one obtains

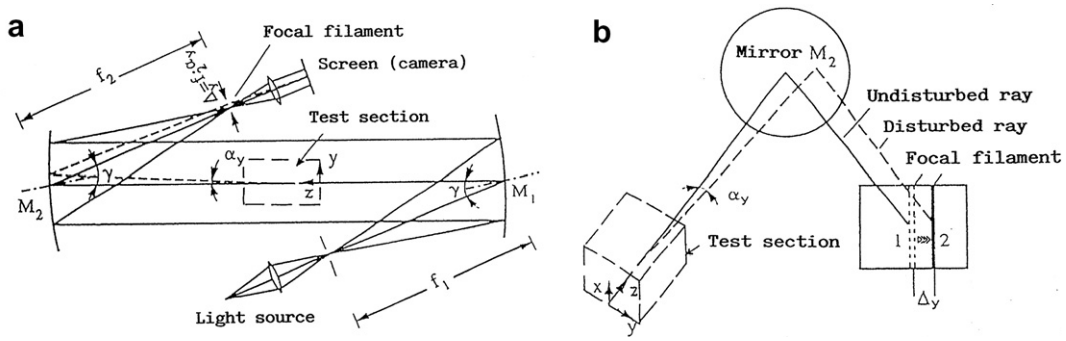

Fig. 3. Schematic layout of the schlieren apparatus: (a) top view, (b) measurement of light deviation in the focal plane of schlieren mirror M_2.

$$\Delta_w = \frac{\Omega}{T_w^2}\left(\frac{\partial T}{\partial y}\right)_w, \quad (2)$$

where $(\partial T/\partial y)_w$ is the fluid temperature gradient, in the direction y normal to the heated plate, evaluated at the wall, and T_w is the wall temperature.

By introducing the local heat transfer coefficient defined as

$$h = -\frac{k_w}{(T_w - T_\infty)}\left(\frac{\partial T}{\partial y}\right)_w, \quad (3)$$

where k_w is the thermal conductivity of the fluid at the wall temperature and T_∞ is the ambient air temperature, it follows that

$$h = -\frac{k_w \Delta_w T_w^2}{\Omega(T_w - T_\infty)}. \quad (4)$$

The uncertainty (at the 95% confidence level) in local heat transfer coefficient h was estimated to range from 8% to 12% in the field of Δ_w values between 9 and 2 mm, in which the majority of measurements were performed. Further details on the derivation of fundamental schlieren formulae as well as of the thermal field reconstruction procedure are given by Tanda (1993) and Devia et al. (1994).

Experimental runs were performed according to the following procedure:

(i) the plate was heated by a given input of electrical power into the heater, in order to achieve the desired uniform temperature over the heated plate;
(ii) at the steady state, measurements of wall and ambient air temperatures were obtained by averaging the readings from the thermocouple arrays deployed in the material and ambient air, respectively;
(iii) for each run the optical measurement of the light deflections at the vertical walls was performed by moving the focal filament in the y-direction, in order to obtain the local heat transfer coefficients at several locations along the vertical surfaces of the heated plate (no h values have been recorded along the rib sides).

3. Results and discussion

3.1. Smooth surface

Local heat transfer coefficients for the unribbed (smooth) vertical surface versus the vertical, upmoving coordinate x, are reported in Fig. 5 for different values of the channel aspect ratio S/H. Inspection of the figure reveals only small differences among the heat transfer coefficient distributions for S/H in the 0.2–0.4 range. As found in the previous papers (Ambrosini and Tanda, 2006; Tanda, 2007) the h values measured for the channel with a sufficiently large spacing are in good agreement (within 15%) with theoretical data obtained by Ostrach (1953) for an isolated (i.e. without shrouding walls), isothermal, vertical surface. Entrance effects are responsible for the larger h values at the leading edge of the heated plate as S/H is progressively reduced from 0.2 to 0.05. For the lowest channel aspect ratio ($S/H = 0.05$) the heat transfer coefficient distribution starts from a very high value at the leading edge but then sharply decreases as the vertical coordinate is increased, owing to the interaction of the growing boundary layer with the unheated facing plate.

3.2. Surface with one rib

When a low-conductivity rib is placed at the middle of the vertical surface, the local distribution of heat transfer coefficient is altered, relative to the smooth surface condition, as shown in Fig. 6 ($S/H = 0.4$). Along the leading region of the plate (and up to about 40% of the height) the h-distribution is coincident with that for the unribbed surface (solid line). A stagnation zone appears to be responsible for the marked reductions in h values immediately upstream and downstream of the rib. Then, the h values suddenly increase up to a relative maximum (approximately located at a distance of $5e$ from the top side of the rib) that exceeds the value recorded for the unribbed plate at the same elevation. This fact is due to the incoming of fresh air induced by the presence of the rib. Beyond this point, h slightly decreases but at a level higher than that of the corresponding value for the unribbed channel.

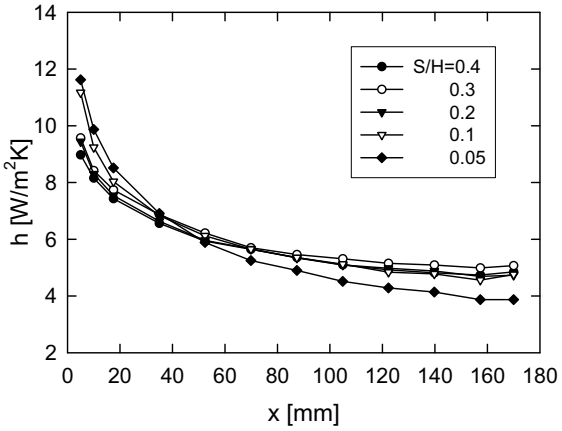

Fig. 5. Heat transfer coefficient along the smooth surface at different values of the channel aspect ratio S/H.

The effect of the channel aspect ratio is depicted in Fig. 7. As the channel aspect ratio S/H is reduced from 0.4 to 0.05, h-distributions exhibit the same behaviour down to $S/H = 0.1$, even though the relative maximum downstream of the rib progressively decreases by a little amount, the location of the maximum remaining the same. At $S/H = 0.05$, the buoyancy-induced flow into the channel is decreased, as occurs for the smooth channel; but here the friction resistances are even higher due to the presence of the rib that locally causes a marked contraction of the free flow area. The h values beyond the rib are not significantly increased (relative to values immediately upstream and downstream of the rib) owing to the relatively low velocity and high temperature of the air washing the wall region downstream of the rib. Moreover, h distribution remains flat up to the trailing edge of the plate.

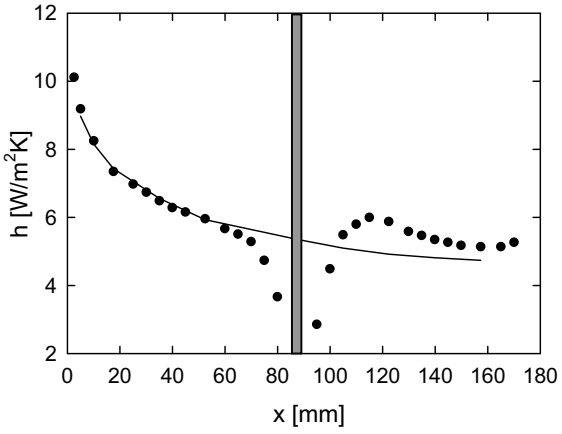

Fig. 6. Heat transfer coefficient along the surface with one rib (symbols) compared with that for the smooth surface (line) for the channel aspect ratio $S/H = 0.4$.

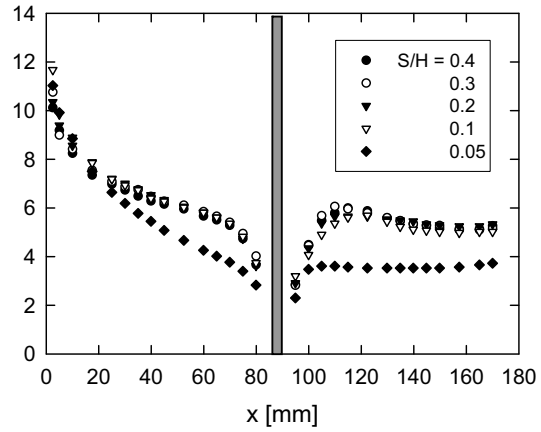

Fig. 7. Heat transfer coefficient along the surface with one rib at different values of the channel aspect ratio S/H.

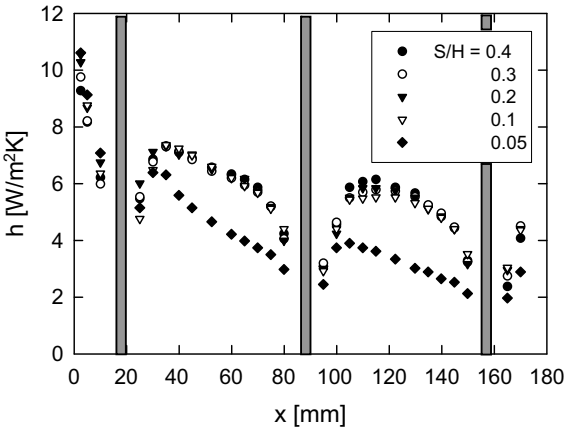

Fig. 9. Heat transfer coefficient along the surface with three ribs at different values of the channel aspect ratio S/H.

3.3. Surface with three ribs

Figs. 8 and 9 show the heat transfer coefficient profiles in the case of three repeated low-conductivity ribs along the heated surface of the channel. The rib pitch P is 70 mm, leading to a rib pitch-to-height ratio $P/e = 14.4$.

For the largest channel aspect ratio ($S/H = 0.4$, Fig. 8), heat transfer coefficients drop to very low values in the vicinity of ribs, and a relative maximum of h is achieved downstream of each rib. The maximum is reached about after $3e$ in the first inter-rib region and after $5e$ in the second inter-rib region. Zones of the surface for which the local heat transfer coefficient is higher than that of the unribbed surface (solid line) account for 50% of the heat transfer area; in the remaining part, h is reduced, even strongly.

Fig. 9 shows the h-distributions at different S/H values. The reduction of the channel spacing from 40% to 10% of the channel height has no impact on the h values between the first and the second rib (from the bottom), while slightly affects the value of the relative maximum along the second inter-rib region (with reductions up to 10%) but not its location. As in the case of the surface with one rib, for the smallest channel aspect ratio ($S/H = 0.05$) the heat transfer is markedly reduced: after a moderate increase in h immediately downstream of each rib, the h-distribution rapidly attains very low values.

3.4. Surface with five ribs

Finally, attention is turned to h-profiles obtained when five low-conductivity ribs are equally spaced over the heated surface. Here the rib pitch P is only 35 mm, yielding a P/e value of 7.2.

For $S/H = 0.4$, the typical inter-rib h-distribution presents a relative maximum (located after $3e$ downstream each rib), whose value progressively decreases as the trailing edge of the surface is approached, as shown in Fig. 10. The stagnation regions that precede and follow each rib occupy a significant part of the inter-rib surface area; for this region values are comparable or lower than those corresponding to the unribbed surface (solid line). It is argued that the ribs are too close to each other to achieve acceptable heat transfer performance (relative to the smooth surface) in the inter-rib regions.

The aspect ratio S/H of the channel does not significantly affect local heat transfer in the 0.2–0.4 range, as shown in Fig. 11. Peaks of lesser magnitude, in the heat transfer coefficient between ribs, are encountered for $S/H = 0.1$ while a general decrease in the heat transfer performance is again observed for $S/H = 0.05$.

From the comparison, shown in Fig. 12, with results obtained by Tanda (1997) for the same geometry and temperature conditions but with high-conductivity ribs, higher inter-rib heat transfer coefficients for the surface with low-conductivity ribs are in evidence at the largest channel aspect ratio ($S/H = 0.4$). This result is

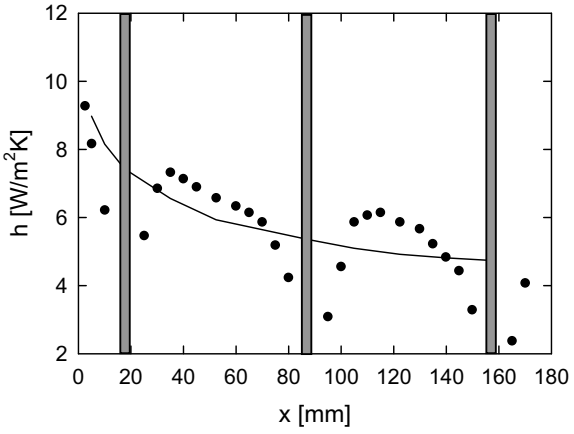

Fig. 8. Heat transfer coefficient along the surface with three repeated ribs (symbols) compared with that for the smooth surface (line) for the channel aspect ratio $S/H = 0.4$.

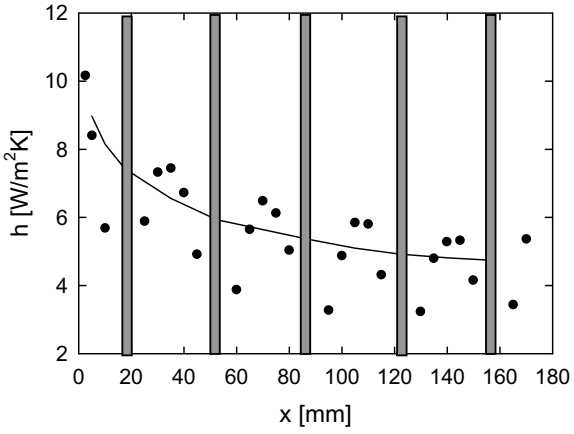

Fig. 10. Heat transfer coefficient along the surface with five repeated ribs (symbols) compared with that for the smooth surface (line) for the channel aspect ratio $S/H = 0.4$.

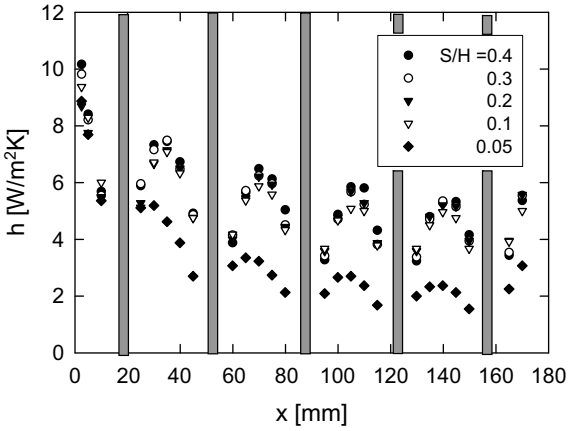

Fig. 11. Heat transfer coefficient along the surface with five ribs at different values of the channel aspect ratio S/H.

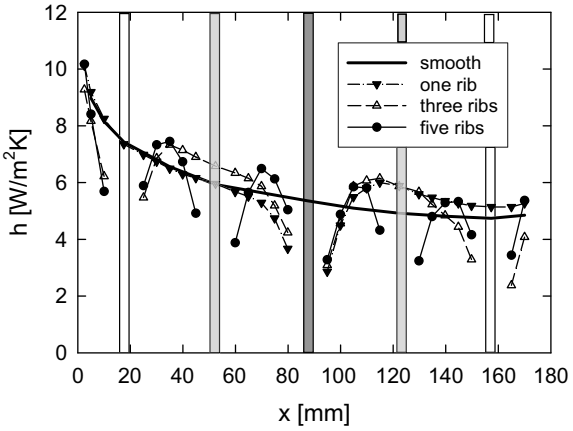

Fig. 13. Heat transfer coefficient along the ribbed (symbols) and smooth (line) surface for $S/H = 0.4$.

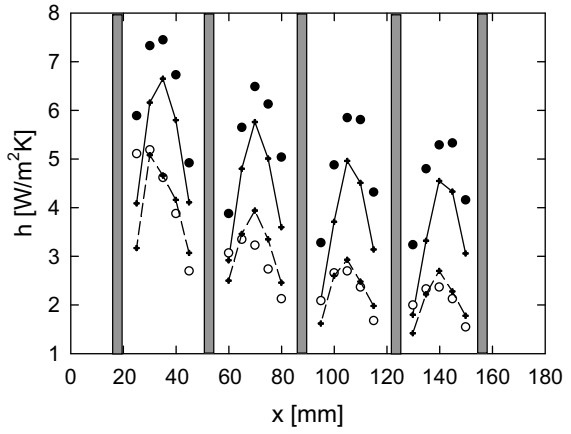

Fig. 12. Inter-rib heat transfer coefficient for the surface with five repeated ribs. Symbols refer to low-conductivity ribs (closed, $S/H = 0.4$ and open, $S/H = 0.05$), lines refer to high-conductivity ribs (data from Tanda (1997): continuous, $S/H = 0.4$ and dashed, $S/H = 0.05$).

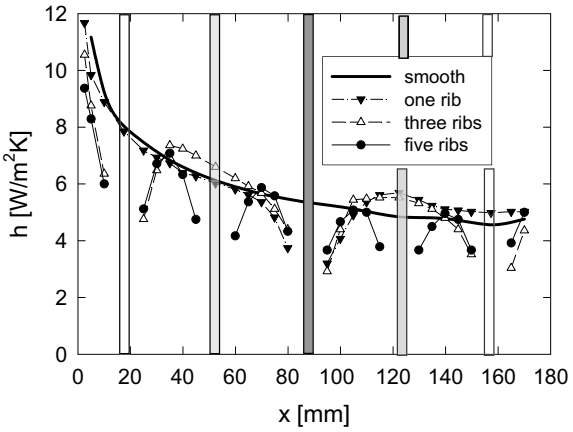

Fig. 14. Heat transfer coefficient along the ribbed (symbols) and smooth (line) surface for $S/H = 0.1$.

consistent with data reported by Bhavnani and Bergles (1990) and can be explained by the development of a less thick thermal boundary layer when the thermal conductivity of ribs is low. Conversely, for the smallest channel aspect ratio ($S/H = 0.05$), levels of heat transfer coefficient in the inter-rib regions are similar, regardless of the value of thermal conductivity of ribs.

3.5. Comparison of heat transfer coefficient distributions for the ribbed surfaces

The heat transfer performance of the vertical surface without ribs and with one/three/five ribs are directly compared in Figs. 13–15.

When the surface is ribbed and the channel spacing is sufficiently large ($S/H = 0.4$, Fig. 13), a significant increase in local heat transfer coefficient (relative to the smooth surface) can be obtained after the stagnation zone immediately following the rib, where a relatively fresh air flow reattaches and a new thermal boundary layer restarts. However, for the three and five ribs cases, the presence of the downstream rib is responsible for premature and marked reduction of the heat transfer coefficient along the inter-rib region.

The reduction in the channel spacing leads to dramatic decreases in local heat transfer. For $S/H = 0.1$ (Fig. 14), only the h-distribution of the one-rib surface is comparable with that of the smooth surface sufficiently upstream of the rib, and even superior sufficiently downstream of the rib. The presence of three ribs yields heat transfer increases in the central part of each inter-rib region, while the heat transfer coefficients of the five-rib surface are typi-

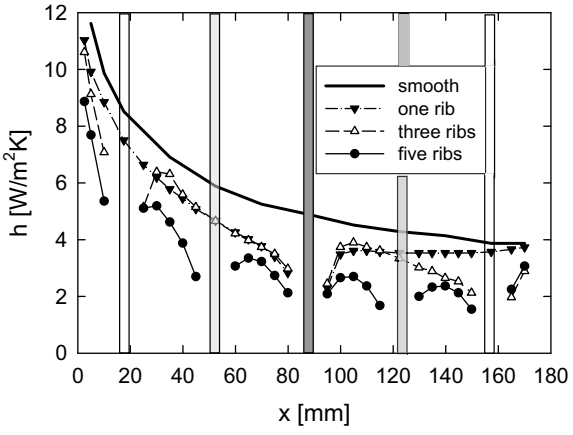

Fig. 15. Heat transfer coefficient along the ribbed (symbols) and smooth (line) surface for $S/H = 0.05$.

cally lower than those of the unribbed plate. For the lowest channel spacing ($S/H = 0.05$, Fig. 15) the heat transfer from the ribbed plates, as compared with that from the smooth plate, is generally reduced and the extent of the reduction increases with the number of ribs.

From the average standpoint, when a single rib is present, the h value integrated over the whole vertical surface does not significantly differ from that obtained for the unribbed surface regardless of the value of the channel spacing, with the only exception of the $S/H = 0.05$, for which the ribs decrease the average heat transfer coefficient by about 18%. Three ribs on the surface cause average heat transfer coefficient reductions from 4% ($S/H = 0.4$) to 9% ($S/H = 0.1$) and to 26% ($S/H = 0.05$). Finally, the average heat transfer of the surface with five ribs is reduced (in comparison with the unribbed surface) from 7% ($S/H = 0.4$) to 15% ($S/H = 0.1$) and to 43% ($S/H = 0.05$).

4. Concluding remarks

An experimental study of natural convective heat transfer inside a vertical, asymmetrically heated, rib-roughened channel has been performed. Ribs, when present, are located on the heated plate of the channel and have low-thermal conductivity, so they do not significantly participate in the thermal exchange with the convective fluid, that is ambient air.

The distribution of the local heat transfer coefficient, measured by the schlieren optical technique, is clearly affected by the presence of ribs on the heated wall; in particular stagnation zones occur immediately upstream and downstream of each rib, with associated low heat transfer coefficients. At a certain distance of the top of each rib, the heat transfer coefficient attains a relative maximum. When the channel spacing is relatively large, the incoming fresh air from the core upmoving current leads to a relative maximum in h value generally higher than that of the smooth surface at the same elevation. However, if the inter-rib distance is too small, the local heat transfer enhancement (relative to the smooth surface) occurs on a little portion of the ribbed surface. As the channel spacing is reduced (from 40% of the channel height to only 5%), the chance for buoyant fresh air to wash the wall downstream each rib is limited due to the reduced amount of air flow drawn into the channel.

When the channel aspect ratio is relatively large (channel spacing equal to 40% of the channel height), the induced flow and thermal conditions are not too far from those corresponding to the isolated (unconfined) vertical plate: in this case, the average heat transfer coefficients for the unribbed and the ribbed surface are comparable when only one rib is present; slight reductions (relative to the smooth surface) within 7% occur when three or five ribs are present. As the channel spacing is reduced (up to only 5% of the height), the heat transfer performance of the ribbed surface (as compared to the unribbed surface) is strongly reduced (from 18% to 43%).

It can be concluded that, in the ranges of parameters here considered, the enhancement of laminar, free convective heat transfer in vertical channels using transverse ribs with low-thermal conductivity can be achieved only locally, at a certain distance downstream of the rib and for not too narrow channels. When repeated ribs are located on the heated plate, the inter-rib distance has to be properly selected in order to prevent the local heat transfer enhancement in the inter-rib region from being offset by the decrease in the stagnation zones immediately upstream and downstream of each rib.

References

Acharya, S., Mehrotra, A., 1993. Natural convection heat transfer in smooth and ribbed vertical channels. Int. J. Heat Mass Transfer 36, 236–241.

Ambrosini, D., Tanda, G., 2006. Comparative measurements of natural convection heat transfer in channels by holographic interferometry and schlieren. Eur. J. Phys. 27, 159–172.

Aydin, M., 1997. Dependence of the natural convection over a vertical flat plate in the presence of the ribs. Int. Commun. Heat Mass Transfer 24, 521–531.

Bhavnani, S.H., Bergles, A.E., 1990. Effect of surface geometry and orientation on laminar natural convection heat transfer from a vertical flat plate with transverse roughness elements. Int. J. Heat Mass Transfer 33, 965–981.

Devia, F., Milano, G., Tanda, G., 1994. Evaluation of thermal field in buoyancy-induced flows by a schlieren method. Exp. Therm. Fluid Sci. 8, 1–9.

Onbaşioğlu, S.U., Eğrican, A.N., 1998. Enhancement of Heat Transfer with Horizontal Promoters, NATO ASI Series E: Applied Sciences, vol. 355. Kluwer Academic Publishers, Dordrecht, The Netherlands, pp. 433–446..

Ostrach, S., 1953. An analysis of laminar free-convection flow and heat transfer about a flat plate parallel to the direction of the generating body force, National Advisory Committee for Aeronautics Report No. 1111.

Settles, G.S., 1985. Colour-coding schlieren techniques for the optical study of heat and fluid flow. Int.J. Heat Fluid Flow 6, 3–15.

Settles, G.S., 2001. Schlieren and Shadowgraph Techniques. Springer, Berlin.

Tanda, G., 1993. Natural convection heat transfer from a staggered vertical plate array. ASME J. Heat Transfer 115, 938–945.

Tanda, G., 1997. Natural convection heat transfer in vertical channels with and without transverse square ribs. Int. J. Heat Mass Transfer 40, 2173–2185.

Tanda, G., 2007. Free-convection heat transfer coefficients along a vertical surface with square protrusions. In: Proceedings of the Vth Baltic Heat Transfer Conference, Saint Petersburg, Russia.